UCRL- 90919
PREPRINT

DAMAGE DEVELOPMENT DURING LOW CYCLE FATIGUE OF CARBON-BLACK LOADED SBR

Donald Lesuer
Alfred Goldberg
David Hiromoto
Lawrence Livermore National Laboratory

Jacob Patt
U. S. Army Tank Automotive Command

This paper was prepared for presentation to the VIII Inter-American Conference on Materials Technology, San Juan, Puerto Rico, June 25-29, 1984

June 18, 1984

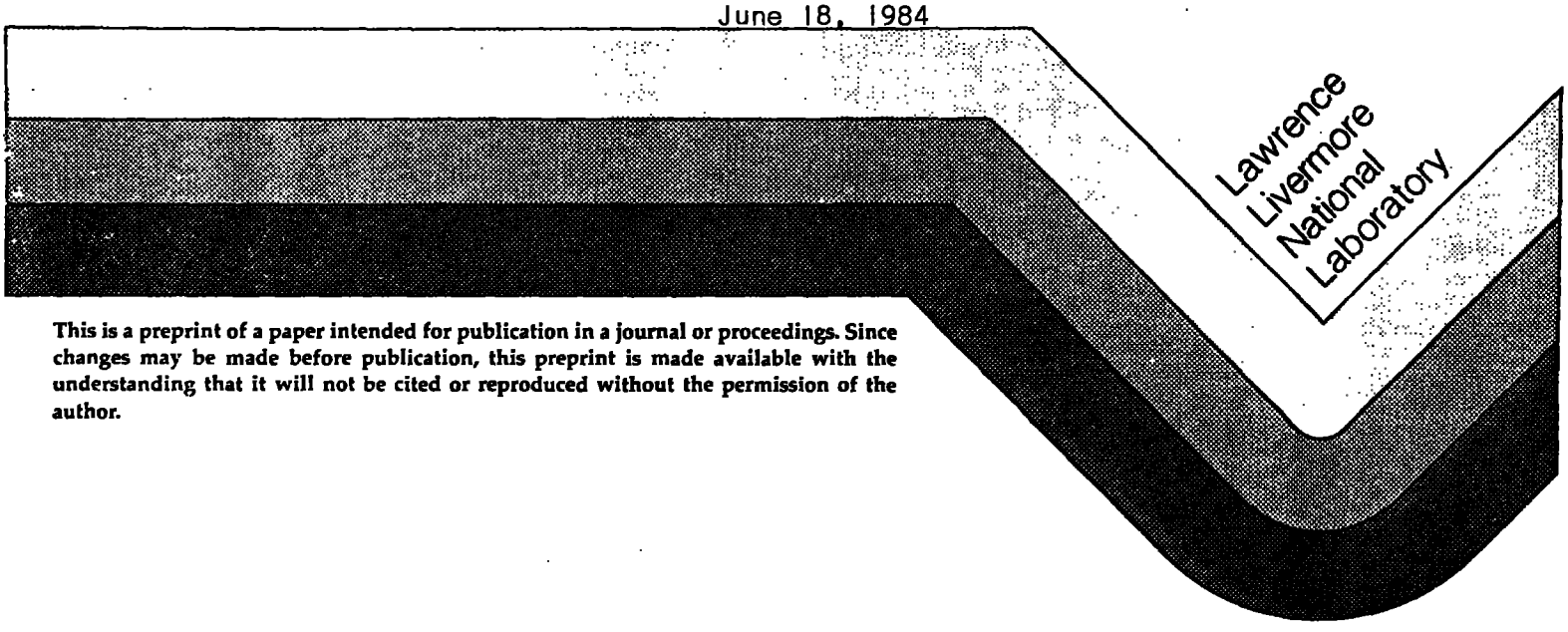

DAMAGE DEVELOPMENT DURING LOW CYCLE FATIGUE OF CARBON-BLACK LOADED SBR*

Donald Lesuer, Alfred Goldberg, David Hiromoto
Lawrence Livermore National Laboratory
Livermore, California 94550

Jacob Patt
U. S. Army Tank-Automotive Command
Warren, Michigan 48090

1.0 INTRODUCTION

Fatigue of elastomers is a subject that has received considerable study over the years (e.g., see Reference 1.) With notable exceptions, most studies have dealt with natural rubber (NR) or styrene butadiene rubber (SBR) without reinforcing filler. In commercial practice, however, most elastomers are used with a carbon-black filler to take advantage of the enormous increases in stiffness and toughness that occur with the use of a filler. In addition, little work has been done on fatigue damage in elastomers in which a limited number of cycles have been applied to the material. Damage can take many physical forms in an elastomer. We use the term in this paper to refer to an irreversible degradation in material properties. In many cases, this degradation can be viewed as a precursor to fracture. This paper explores the problem of damage accumulation in a series of SBR based compounds containing 0, 15, 25, and 35 weight percent carbon-black under conditions in which a limited number of higher stress cycles have been applied to the material (referred to here as low cycle fatigue.)

2.0 EXPERIMENTAL

2.1 Materials

Formulations for the four SBR based elastomers used in this study are given in Table I. The notation used for the various formulations is included. It is important to recognize that the formulations are identical except for the amount of carbon black. Thus, the polymer phase of the various compounds possesses the same structure (i.e., identical cross-link density, cross-link type, molecular weight, etc.) The only variable between compounds is the amount of hard reinforcing, carbon-black phase.

---

* Work performed under the joint auspices of the U. S. Department of Energy by the Lawrence Livermore National Laboratory under Contract W-7405-ENG-48 and the U. S. Army Tank-Automotive Command.

TABLE I

FORMULATIONS OF SBR SAMPLES

INGREDIENT	phr	INGREDIENT	phr
SBR 1500	100	CBS Santocure	1.0
Sulfur	1.75	Octamine	1.0
Stearic Acid	2.0	Dutrex 726	6.0
Zinc Oxide	5.0	HAF Black-N330	Variable

Carbon Black

DESIGNATION	phr	Wt. %
SBR-0	0	0
SBR-15	20.6	15
SBR-25	38.9	25
SBR-35	62.9	35

2.2 Testing

Our testing objective was to quantitatively evaluate the extent of damage development due to fatigue. Experimentally, this evaluation had a two-step procedure. The first step was to fatigue the material by cyclically loading a sample in an MTS Servo-Hydraulic Test Machine between zero and some predetermined load at 1 hertz for 100 cycles. The stress produced by this predetermined load will be referred to as the cycling stress. Testing was done on flat, dog-bone shaped samples that were die-cut from a vulcanized sheet of rubber. The second step in this procedure was to pull the sample to failure. This was done immediately after cyclic loading. The ultimate tensile strength measured in this test will be referred to as the residual strength, and can be used as a measure of the damage developed in the material due to fatigue loading. After testing, the fracture surfaces were examined using both optical and scanning electron microscopes.

3.0 RESULTS AND DISCUSSION

3.1 SBR Without Carbon Black

Results for SBR without carbon-black (plotted as residual strength versus cycling stress) are presented in Figure 1 for testing temperatures for 22 and 60° C. Notice that for 22° C, the material shows little damage or degradation until a critical cycling stress (damage threshold) is reached. At this stress, severe degradation occurs with obvious incipient failure. Notice, that increasing the testing temperature decreases this damage threshold. Also, at 60° C measurable degradation occurs even at small cycling stresses well below the threshold.

The results reported above can be analyzed further by deriving the relationship between the cycling stress and residual strength for the test described earlier. For many different materials, the fatigue crack growth rate (dc/dN) can be represented by the relationship

$$dc/dN = A(\Delta G)^n , \qquad (1)$$

where:

c	=	length of a cut or flaw
N	=	number of cycles
ΔG	=	change in strain energy release rate
A	=	constant
n	=	constant

For the case of a rubber strip loaded in uniaxial tension, the strain energy release rate, G, for flaws has been shown to be given by the expression

$$G = 2BCW , \qquad (2)$$

where W is the strain energy density in the absence of a flaw and B is a constant. The length of a flaw in a rubber strip subject to fatigue can be obtained by substituting Equation 2 into Equation 1 and integrating. The result is

$$c = [(-n + 1)\, A\, (2B\Delta W)^n\, N + C_o^{(-n+1)}]^{1/(-n+1)} \qquad (3)$$

where C_o is the initial flaw size and ΔW is the cycling strain energy density. Equation 3 represents the flaw length after the fatigue loading described earlier. The critical strain energy density, W_c, required to produce fracture is then given by

$$W_c = \frac{G_c}{2B}[(-n + 1)\, A\, (2B\Delta)^n\, N + C_o^{(-n+1)}]^{1/(n-1)} \qquad (4)$$

where G_c is the critical strain energy release rate for fracture. The parameter G_c was evaluated independently from experiments in cut rubber strips and was determined to be 2409 J/m^2 (13.8 in lb/in^2.) The relationship between W and the applied tensile stress was obtained experimentally from a uniaxial tensile test.

Plots of residual strength versus cycling stress obtained from Equation 4 are presented in Figure 2. Data derived experimentally is shown in the figure. The constants A and n, 3.5 x 10^{-19} $m(Jm^{-2})^{-4}$ and 4, respectively, were chosen to best fit the experimental data. B was assumed to be 1.7.[2] The agreement between the theoretical results and experimental data is excellent. The constants, A and n, are very similar to values obtained in cut growth experiments[3], 10^{-18} $m(Jm^{-2})^{-4}$ and 4, respectively, in which the growth of deliberate razor cuts in fatigue was studied over a wide range of strain energy release rates. Thus, it appears that the damage accumulation experienced in unloaded SBR at the conditions described above is by flaw growth from flaws initially present in the elastomer. The initial flaw size was found to be 102 μm. Also, shown in Figure 2 is the variation of residual strength with cycling stress that would be obtained for initial flaw sizes of 150 and 200 μm. The size of the critical flaw after the fatigue loading is also shown in the figure. The material experiences very little damage or flaw growth until cycling stresses very near the damage threshold are applied. One would observe a similar result if the residual strength was examined as a function of the number of applied cycles for a given cycling stress. For this problem, little crack growth is observed for most of the sample lifetime.

It is informative to compare these results on damage accumulation in fatigue with results on damage accumulation under creep-rupture conditions using a kinetic theory of crack growth.[4] In the later study, the material was assumed to be subjected to constant stress for an arbitrary time. Little degradation of the material is observed until the time of load application was close to the ultimate lifetime under the given applied load. Thus, in both creep and fatigue, if flaw growth is the predominate damage mechanism, then little damage accumulation occurs unless test conditions are near the damage threshold.

3.2 SBR With Carbon Black

In Figure 3, we present the results for SBR-35 w/o carbon black at temperatures of 22, 60, 100, 120, and 140° C. The results at 22° C show the same trend as results at 22° C for unloaded SBR -- little damage is experienced unless experimental conditions are near the damage threshold. However at 60, 100, and 120° C, results show increasing deviation from threshold phenomena. In fact, attempts to fit the experimental data with Equation 4 (using reasonable values of the growth law constants A and n) were unsuccessful. The strong non-linear dependence of flaw size on cycling strain energy density provides for threshold-like behavior with all reasonable values of n. Thus, the power-law form for the fatigue crack growth rate is unsatisfactory and one would suspect that damage accumulation occurs by some mechanism other than or in addition to flaw growth. One should notice that at 100° C, the damage curves for unloaded and loaded SBR exhibit a similar shape. This suggests that the changes in damage mechanism that occur with increasing testing temperature are occurring in the polymer phase.

In Figure 4, we show the influence of increasing carbon black content on the residual strength versus cycling stress behavior. Results are presented for SBR-15, SBR-25, and SBR-35 at 100 and 140° C. From Figure 4, one can see the enormous effect that carbon-black has on raising the damage threshold. Comparing Figures 1 and 3, one can see that adding 35 w/o carbon-black raises the damage threshold by over a factor of 10 relative to the unloaded SBR.

4.0 FRACTOGRAPHIC OBSERVATIONS

4.1 Overview

Fractured surfaces of a large number of samples were examined with emphasis on SBR-35, our formulation that comes closest to those used in U.S. Army tank track pads. The SBR-35 samples, tested at 22, 100, and 140° C, were evaluated using both light microscopy (LM) and scanning electron microscopy (SEM), while SBR-15 samples tested at 100 and 140° C were examined using only LM. The initation sites, the fatigue or slow crack-growth regions, and the catastrophic crack-growth regions were evaluated and compared. With rare exceptions, tearing was always initiated at a (bulk) material flaw in contrast to a (surface) mechanical flaw. However, no correlation was found to exist between the extent of cyclic damage and flaw size. This is consistent with the observations reported by Morgan, et al., on initiation sites for failure in amine-cured epoxies[5]. The initiation flaws and the contiguous fatigue or slow crack-growth regions are clearly visible in the SBR-35 samples where the flaw sizes are of the order of 50 to 200 μm. The initation flaws are generally smaller and less clearly defined in the corresponding fractured SBR-15 samples, although the initiation sites are equally visible. We also examined the initiation flaws in SBR-0 samples tested at 22° C and these were found to be still smaller than those in samples of either SBR-35 or SBR-15, and again there was no direct bearing between the extent of damage and flaw size. Furthermore, the morphology of the flaws varied considerably, again without any apparent effect on properties. However, some general trends in the morphological tearing and fracture feature can be related to the extent of cyclic damage in terms of either an increase in cyclic stress or a decrease in residual strength for a constant cycling stress. These trends are most clearly revealed at the lower magnifications. However, details of the initiation sites (flaws) can only be seen at high magnifications and these are discussed first below. High magnification SEM views, focused on initiation sites, are shown in Figures 5 through 8. Figures 9, 10, 11, 13, and 14 are low magnification views (both LM and SEM) that address the concentric bands, slow crack growth, and fast crack growth. Details of the tearing in both the slow and fast crack-growth regions are shown in the SEM views of Figures 8 and 12.

4.2 Initiation Sites in SBR-35

Figures 5, 6, and 7 contain random examples of initiation tearing sites for SBR-35 samples tested at 22, 100, and 140° C. The SEM views shown were taken at magnifications of 1 kX (upper views) and 10 kX (lower views). As can be seen, both the shapes and morphologies of the flaws vary. One may speculate as to the origin of these flaws: foreign particles, improper mixing, curing defects, gelled material, antioxident by-products, etc. Energy dispersive spectrographic (EDS) analysis of several samples did not reveal any significant difference between the flaws and other regions; both showed only sulfur and zinc peaks. Some of these flaws were also observed in fractured samples without prior cycling; e.g., similar to those seen in Figures 7 (a) and (c).

Some of the flaw features seen at 10 kX correspond to frequently observed tearing morphologies; e.g., Figures 5 (c) and 7 (d), and to a lesser extent, 6 (d) are typical of morphologies present in slow crack-growth regions (contiguous with initiation sites). Indeed, in each of these samples the flaw appears to have been pulled out or fallen out, indicating that we are now viewing the surface interface that had contained the flaw. In Figures 6 (a) and (c) it appears that the flaw has been pulled apart in a taffy-like manner. The crazed pattern shown in Figures 5 (b) and (d) suggests cracking and this may be indicative of some heterogeneity with low ductility; e.g., a region of excessive cross linking due to high sulfur or alternatively an excess of carbon black. The small spheres (< 1 μm) shown in Figure 7 (c) were observed in a number of samples in regions outside of the initiation site, but usually as isolated spheres. Some initiation sites revealed clusters of such spheres, while a few consisted entirely of these spheres.

Figure 8 (a) is an SEM fractrograph taken at 1 kX of a sample of SBR-35 that failed during the tenth cycle at 100° C and on which the fracture apparently was initiated at some surface defect, e.g., a nick. Views (b) and (c) were taken at 10 kX and show structures typical of slow-growth and rapid-growth regions, respectively; view (b) was taken at the initiation site, shown in (a), while view (c) was taken at some distance (≈ 1 mm) outside of the field shown in (a). This sample is also shown in Figures 10 (c) and 11 (b). At 1 kX and 10 kX it is apparent that the fracture surface is initially relatively rough and becomes continuously smoother as it progresses from the initiation site into the fast-fracture region. This is discussed in more detail below.

4.3 Crack-Growth Morphologies in SBR-35 at Low Magnifications

Figures 9 and 10 are low magnifications (13.1 X) LM views of SBR-35 samples cycled and fractured at 22 and 100° C, respectively. The sequence of views (a) through (e) in Figure 9, and (a), (b), (c) in Figure 10, represent increasing cyclic stress, while views (f), (g), (h) in Figure 9, and (d), (e), (f) in Figure 10, represent an increase in fatigue damage (loss of residual strength) for a given cyclic stress. The morphological features that show similarities are as follows: Usually only an initiation site could be detected. An exception to this is shown in Figure 9 (c) which reveals at least three such sites (S). The initation sites are enveloped by a fan-shaped or penny-shaped area consisting of one or more concentric bands, suggesting that the crack (tear) growth radiates out uniformally from the initiation source. These bands are generated by the discontinuous growth of the flaw during fatigue loading. Where there are a number of such bands, the bands usually become progressively wider with growth of the crack (see Figures 9 (e), 9 (h), 10 (c), and especially the views in Figure 11). This behavior is consistent with that of an increase in stress concentration with crack growth. The boundary outlining the banded region indicates a major change in tearing rate; tearing probably becomes catastrophic at the point. The number of concentric bands increase with an increase in cycling stress while the banded areas become more clearly defined with either an increase in stress or an increase in damage at constant stress. At this magnification it appears that the fracture is relatively smooth within the bands and generally relatively rough in the fast fracture region, the reverse of what is observed at high magnifications. The roughness is clearly due to tearing occurring along different fracture paths. At high magnification, individual smooth fracture paths are observed in the fast-fracture regions, except when one focuses on a ledge between such paths. As the temperature increases, the effect of knotty tearing (the discontinuous tearing along directions deviating significantly from the normal to the tensile axis) is superimposed on these features. At 100° C, tearing is initiated by the formation of a dome-like surface due to such tearing. Figure 1 contains SEM fractographs of three SBR-35 samples cycled at near threshold stresses at 22, 100, and 140° C. Two effects are seen; both the number of discontinuous crack-growth regions (fatigue bands) and the influence of knotty tearing increase with an increase in temperature. At 140° C, the knotty tearing becomes very prevalent and causes difficulties with focusing using LM; near the initiation site, extensive tearing has occurred along directions approaching the tensile axis.

The size of the banded areas (in contrast of their sharpness) appears to be independent of either the cycling load or the degree of damage at constant load. Also, no significant trends are apparent external to the band regions. Series of fine lines may be seen radiating out from either the initiation source or the boundary of the banded region. These lines represent tearing along finely separated planes. At somewhat higher magnification these regions are seen to consist of connecting "links" suggesting the sequential tearing of clusters of molecular chains (see Figures 11 (a) and 12 (a). The appearance of ledges indicates increased displacement between fracture paths, while the rough nodular-like regions probably represent large clusters of molecular chains tearing at different levels along the fracture path. In Figure 9 (c), one can see some indication of initiation sites at the origin of three tear paths (Y). This is consistent with suggestions frequently made that tearing is often initiated at distinct defects ahead of the main fracture front. The magnitude of the ledges between fracture paths in the fast crack-growth regions appear to increase with increasing cyclic stress or cyclic damage, but only at the higher temperatures of 100 (see Figure 10) and 140^{o} C and this may be related to the knotty tearing in the preceding slow crack-growth regions.

4.4 Crack-Growth Morphologies in SBR-35 at High Magnifications

Figure 12, contains SEM fractographs which illustrate the changes in morphology seen at high magnification in the banded regions. View (a) shows a number of bands, at least 8, surrounding the flaw (F) for a sample that failed after 83 cycles at 22^{o} C. View (b) was taken in a region just above F, contiguous with the flaw. One may note rough, plate-like nodules containing clusters of much smaller disk-shaped cells ≈ 1 μm in size; both represent the collapsing of large and small groups of torn molecular chains, respectively. Fracture paths are frequently indicated by the long axis of the larger nodules. This morphology remains essentially unchanged (perhaps a slight decrease in roughness) in passing from inner to outer bands. View (c) is at the interface of the band area/fast-fracture region indicated by I. The structure suddenly becomes much smoother; the plate-like nodules disappear. However, the small individual cells are still present suggesting that these represent a basic group of tearing units along a local planar fracture path. Views (d) and (e) are fractographs taken adjacent to the initiation flaws of

sample cycled at 100 and 140° C, respectively. Two observations can be made; the larger plate-like nodules are absent and a porous-like structure appears in the matrix emphasizing the individual disk-shaped cellar units. The latter becomes more prevalent with an increase in temperature change in morphologies with temperature. This is consistent with the effect of tearing rate on morphology in SBR-35[6]. It is as if the tearing of these basic cellular units in this formulation becomes more and more mutually independent with an increase in temperature or a decrease in strain rate. The irregular ridges seen here result from tearing along adjacent tear paths. The morphology in the fast-fracture regions is similar for all three temperatures. The tearing/fracture features described for each of the temperatures are typical of all samples examined at the respective temperature, independent of cyclic stress or the extent of fatigue damage.

4.5 Morphologies in Fractured SBR-15

The fractographs taken (13.1 X) of SBR-15 samples cycled at 100 and 140° C are shown in Figures 13 and 14, respectively. In both figures, the sequence of views (a), (b), and (c), and (d), (e), and (f) corresponds to increasing cyclic stresses. The two sequences represent samples with minimum and maximum cyclic damage, respectively, at the same corresponding cyclic stresses. In both figures, views (a) and (d) refer to samples with no prior cycling, i.e., zero cycling stress. Both similarities and differences may be noted between the SBR-15 and SBR-35 samples. As with SBR-35, usually only one initiation site can be seen and these are mostly at material flaws. The initiation sources also are enclosed by penny- or fan-shaped bands; but here they are all single continuous bands, suggesting that the fatigue tearing in SBR-15 is of a much more continuous nature than that occurring in SBR-35. As with SBR-35, both the initiation site and the contiguous slow-growth region become more clearly defined with either an increase in cyclic stress or an increase in damage at constant stress. In addition, however, the fast-fracture regions become rougher with deeper ledges as either the cyclic stress or the degree of damage increase. We also see a general trend of an increase in the area of the slow crack-growth (band) region; this suggests that the slow crack-growth region, which develops before catastrophic failure is initiated, is larger as either the cyclic stress or fatigue damage increases. This is consistent with observations that we have made on the effect of cut size on cut growth in SBR-15 samples, in that the fracture surface becomes rougher with an increase in cut depth.

4.6 Discussion on Fractographic Observations

In the absence of mechanical surface defects, tearing is always initiated at some material flaw. Usually, only one such flaw is detectable. However, the extent of cyclic damage cannot be related to either the flaw size or flaw morphology. In addition, the fine details of the tear surfaces in regions contiguous with the flaws are similar at a given temperature, and vary only with temperature. Nevertheless, the nature of the flaw or the contiguous surroundings must influence, in some way, the initiation of tearing. Differences might be revealed with the use of more sophisticated analysis, such as with ESCA.

Initiation sites are enveloped by penny- or fan-shaped regions. In SBR-35, these regions often consist of a number of concentric bands. By contrast, these bands are absent in the corresponding regions of SBR-15 and SBR-0 samples. This difference may be due to the tendency for knotty tearing in the former samples which is likely to introduce disorientation between consecutive tearing cycles. Consistent with this suggestion is that a simultaneous increase in banding and knotty tearing occurs with an increase in test temperature. In a separate paper[7] we noted that for nicked tensile-tested samples, the ratio of the strain required to initiate tearing to that at failure decreases with increasing carbon-black content. Thus, alternatively, the absence or presence of concentric bands may be related to the ratio of critical damage at the root of the flaw (nick) necessary to initiate cyclic tearing to that necessary for initiating catastrophic crack growth. The lower this ratio, the greater will be the cyclic tearing before final failure. This is consistent with the concept of a narrow critcal damage limit or a narrow band of crack length increase with cycling.

The penny- or fan-shaped band regions become more clearly defined with an increase in cyclic damage; but the size of these regions is independent of such damage. In samples that have suffered only slight cyclic damage, the slow crack-growth region experiences additional growth during subsequent loading to failure. By contrast in severely damaged samples the fast (catastrophic) crack-growth may have been initiated immediately on reaching a critical number of loading cycles or on reloading to failure after the 100 cyles. This may account for the variability in the slow crack-growth areas.

In, at least, the more severely damaged SBR-35 samples, the width of the concentric bands increases with the propagation of fatigue tearing right up to the outer band, and this is consistent with an increase in stress concentration with crack depth.

The suggestion of critical damage accumulation cycles at the crack tip is also inconsistent with the morphological features seen at high magnification in the banded region. These features are independent of the degree of damage and are only dependent on the cyclic test temperature.

We do not understand why there are differences in the relative size of and/or the ability to detect critical flaws in the three elastomers examined. It appears that the samples with the highest carbon-black content have the greatest tendency of the three elastomers to initiate tearing at material flaws in contrast to surface (mechanical) flaws. This is consistent with the material flaws being larger in the SBR-35. Is this due to the higher carbon-black content aiding the development of flaws in the compounding/curing process, or is it that the knotty tearing exaggerates the presence of the flaw? In tensile tests with nicked samples, crack growth is initiated at continuously higher strains with increased carbon-black contents up to about 30 wt% carbon black; accordingly, the degree of crack blunting, before crack initiation, would be greatest for the higher carbon-black loaded material. It is possible that this extra blunting of mechanical surface defects may favor tear initiation from a material flaw.

5.0 SUMMARY AND CONCLUSIONS

Damage development in elastomers can take many forms. Generally speaking, one can classify the degradation as mechanical or chemical in origin. The most obvious form of mechanical damage is flaw or cut growth, while typical examples of chemical damage include chain scission or thermal oxidation. The fatigue crack growth relationship given in Equation 1 obviously only applies to flaw growth. However, it does an excellent job of following the data and exhibits the threshold behavior observed in both SBR and SBR-35 at room temperature. At higher temperatures, the damaged material shows an increasing deviation from threshold behavior. The obvious implication is that some thermally activated damage mechanism is degrading the material.

In previous work, carbon-black loaded SBR subjected to a high temperature, high stress environment was shown to undergo a thermal-mechanical oxidation process. Certainly, this process is a candidate for a damage mechanism in these studies.

6.0 REFERENCES

1. Gent, A. N., "Science and Technology of Rubber," Eirch, F. (ed), Academic Press, New York, Ch. 19, p. 419.

2. Greensmith, H. W., Journal of Applied Polymer Science, V 7, 1963, p. 993.

3. Lake, G. J. and Lindley, P. B., "Cut Growth and Fatigue of Rubbers. II. Experiments on a Noncrystallizing Rubber," Journal of Applied Polymer Science, V 3, 1964, pp. 707-721.

4. Christensen, R. M., "Residual Strength Determination in Polymeric Materials," Journal of Rheology, V 25, 1981, pp. 529-536.

5. Morgan, R. J., Mones, E. T., AND Steele, W. S., "Tensile Deformatin and Failure Processes of Amine-Cured Epoxies," Polymer, V 23, 1982, pp. 295-305.

6. Goldberg, A, Lesuer, D. R., Stone, J. C., and Patt, J., Paper in preparation.

DRL:AG:MDM
0849M

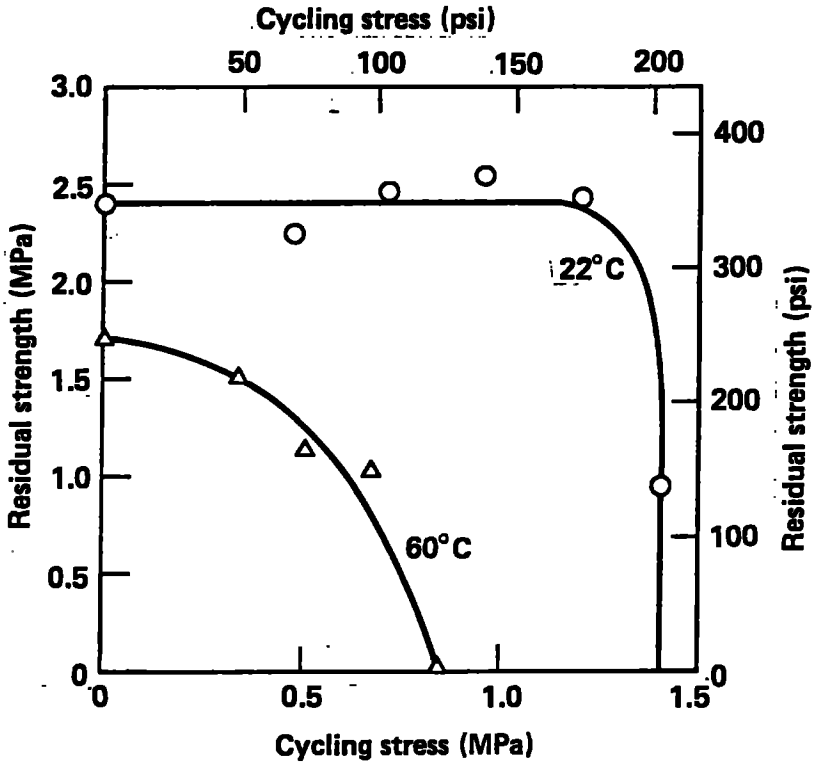

Figure 1: Residual strength versus cycling stress for SBR-0 at 22 and 60° C

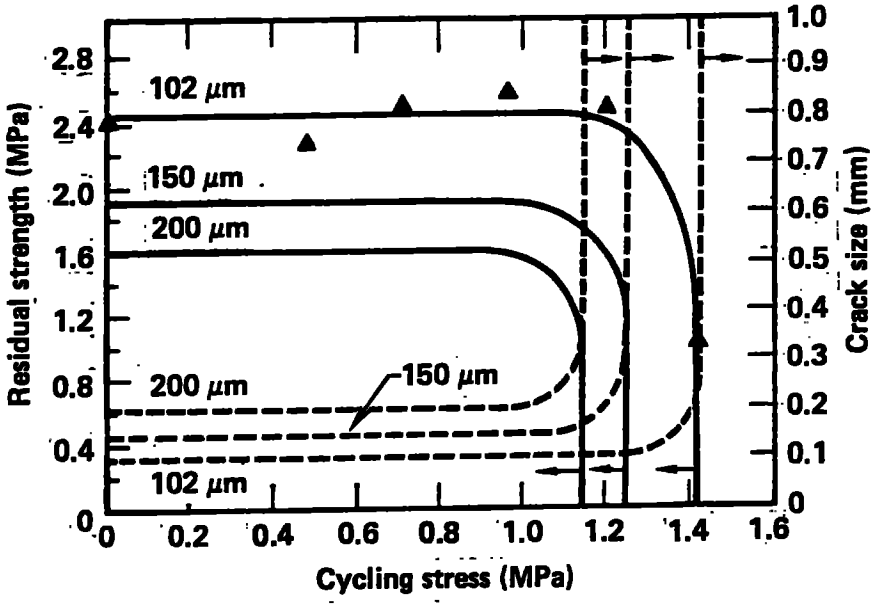

Figure 2: Residual strength versus cycling stress derived from Equation 4 for three different initial defect sizes (as solid curves.) Experimental data points for SBR-0 at 22° C are shown in the figure. The size of this initial flaw after the fatigue loading is also shown in the figure (as dashed curves)

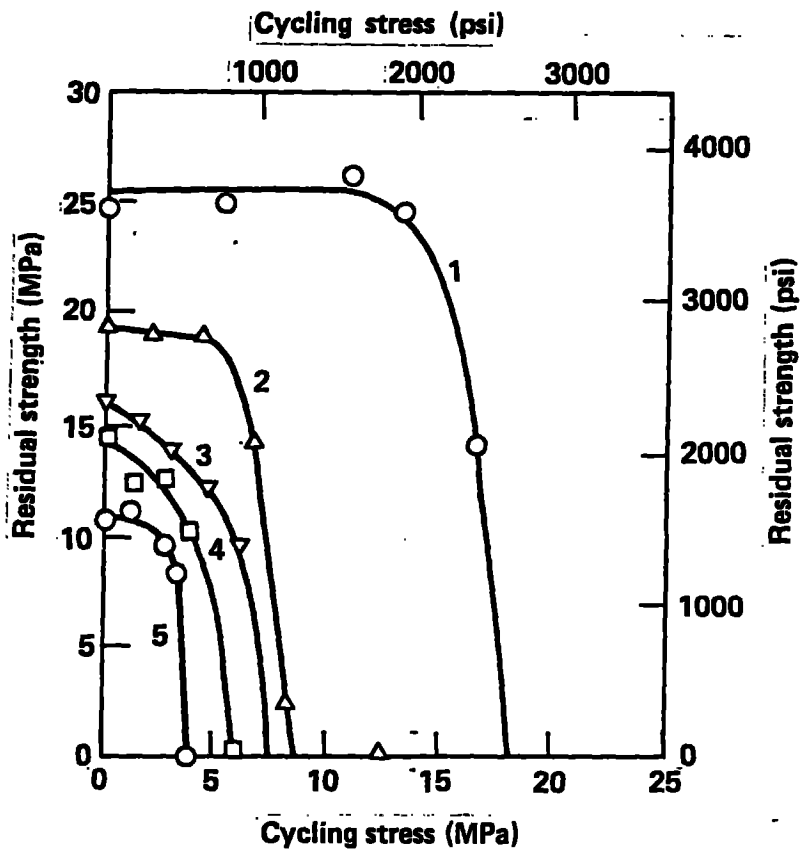

Figure 3: Residual strength versus cycling stress for SBR-35 at 22° C (Curve 1), 60° C (Curve 2), 100° C (Curve 3), 120° C (Curve 4), and 140° C (Curve 5)

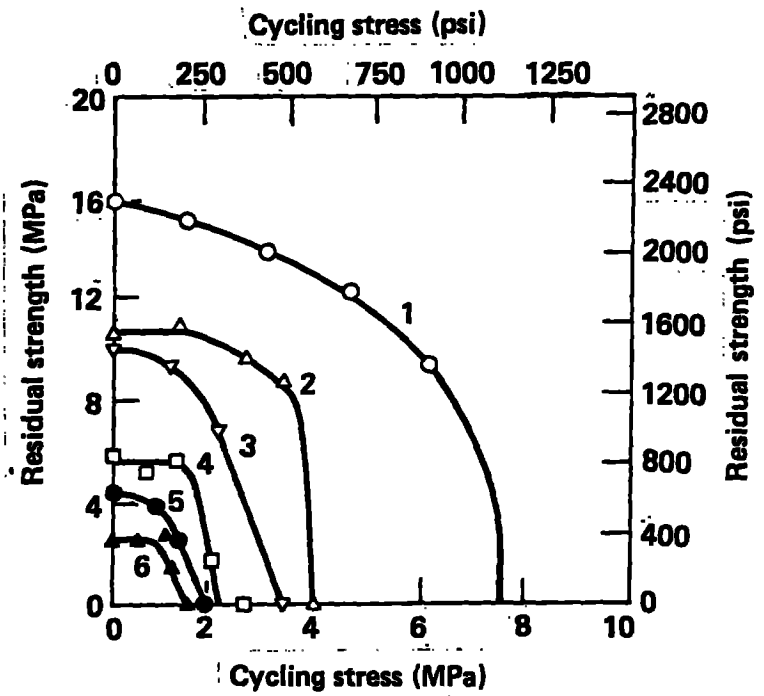

Figure 4: Residual strength versus cycling stress for SBR-15, SBR-25, and SBR-35 at temperatures of 100 and 140° C. Test temperatures and material tested are identified as follows: (1) SBR-35 at 100° C; (2) SBR-35 at 140° C; (3) SBR-25 at 100° C; (4) SBR-25 at 140° C; (5) SBR-15 at 100° C; (6) SBR-15 at 140° C

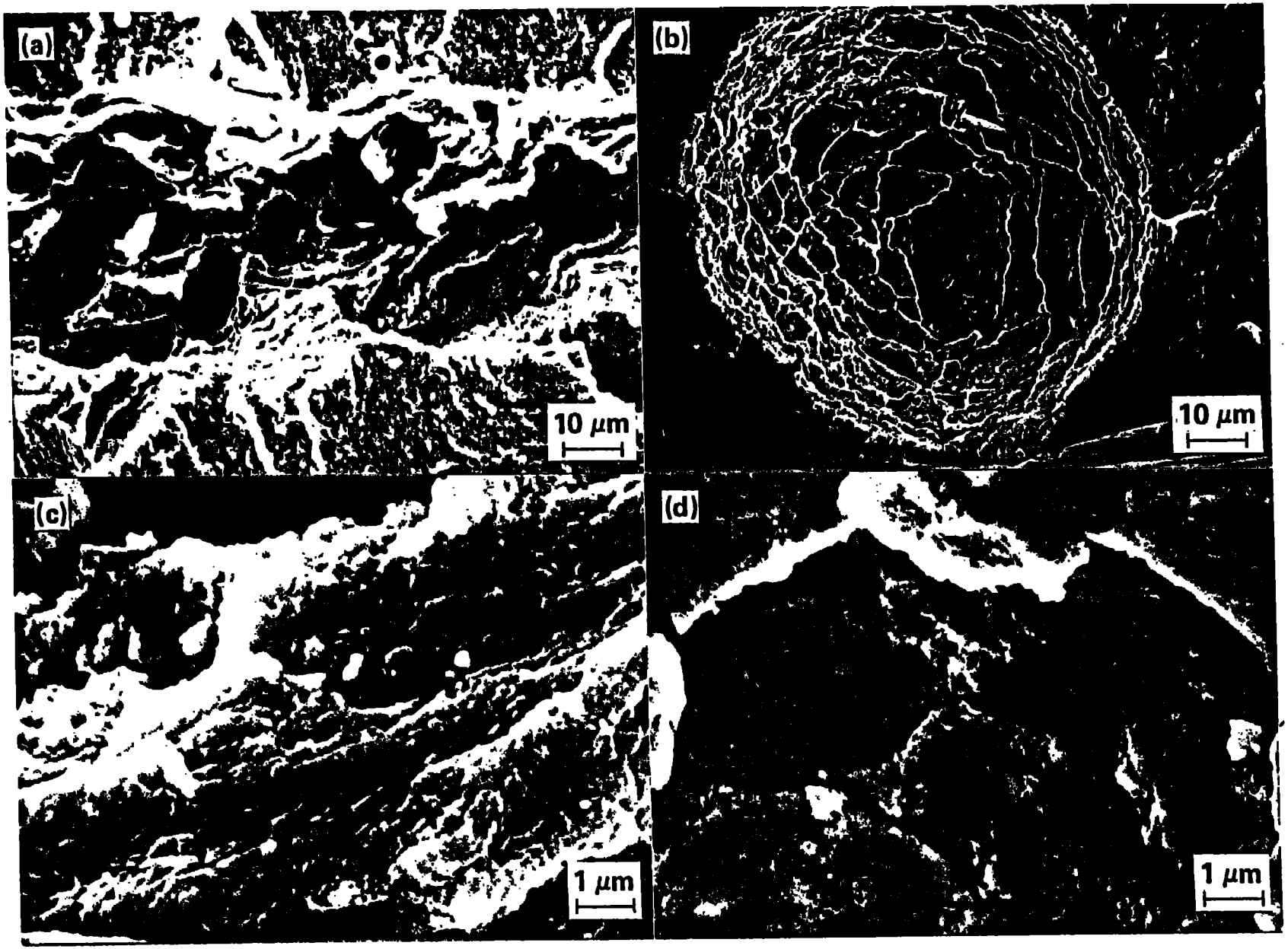

Figure 5: Initiation flaw sites of SBR-35 samples cycled at 22° C: (a) 83 cycles at 0 to 16.8 MPa (2.44 ksi) — failed on cycling; (b) 100 cycles 0 to 16.5 MPa (2.39 ksi) — residual strength of 18.2 MPa (2.64 ksi)

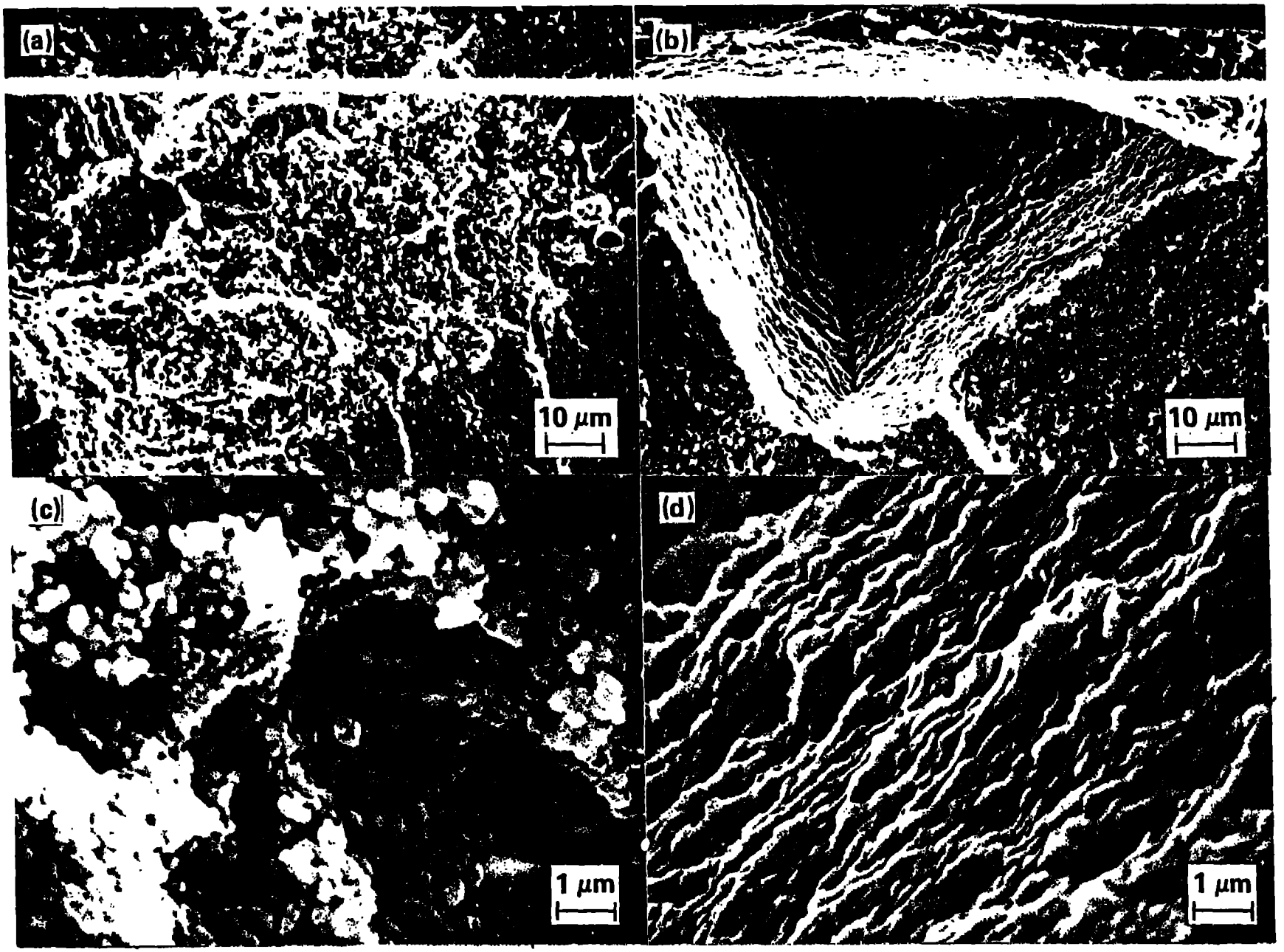

Figure 6: Initiation flaw sites of SBR-35 samples cycled at 140° C: (a) 100 cycles at 0 to 2.92 MPA (0-424 psi) — residual strength of 14.2 MPa (2.06 ksi); (b) 100 cycles at 0 to 6.08 MPa (882 psi) — residual strength of 11.2 MPa (1.63 ksi)

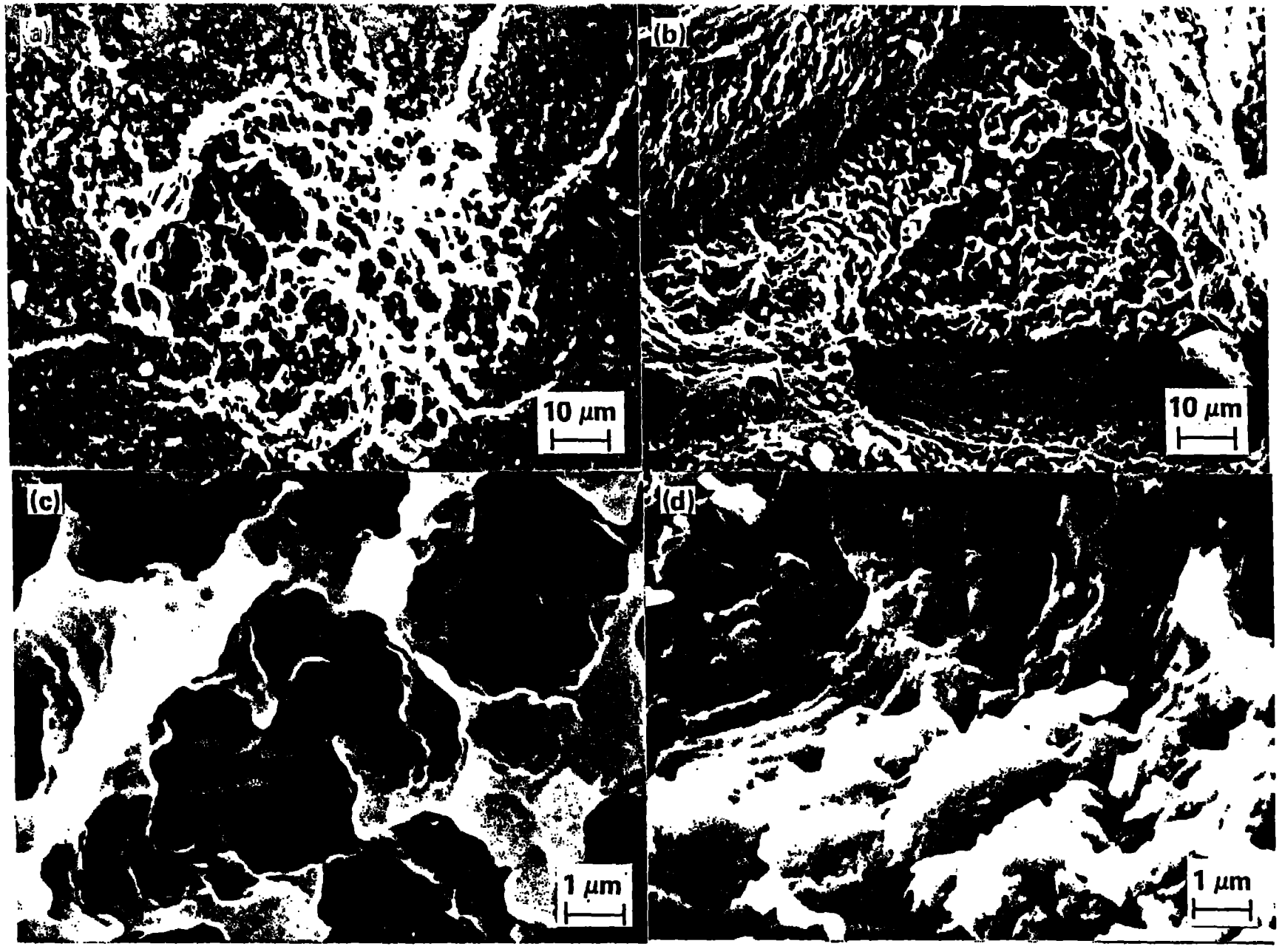

Figure 7: Initiation flaw sites of SBR-35 samples cycled at 100° C: (a) 90 cycles at 0 to 3.79 MPa (550 psi) — failed on cycling; (b) 100 cyles at 0 to 1.25 MPa (181 psi) — residual strength of 10.89 MPa (1.58 ksi)

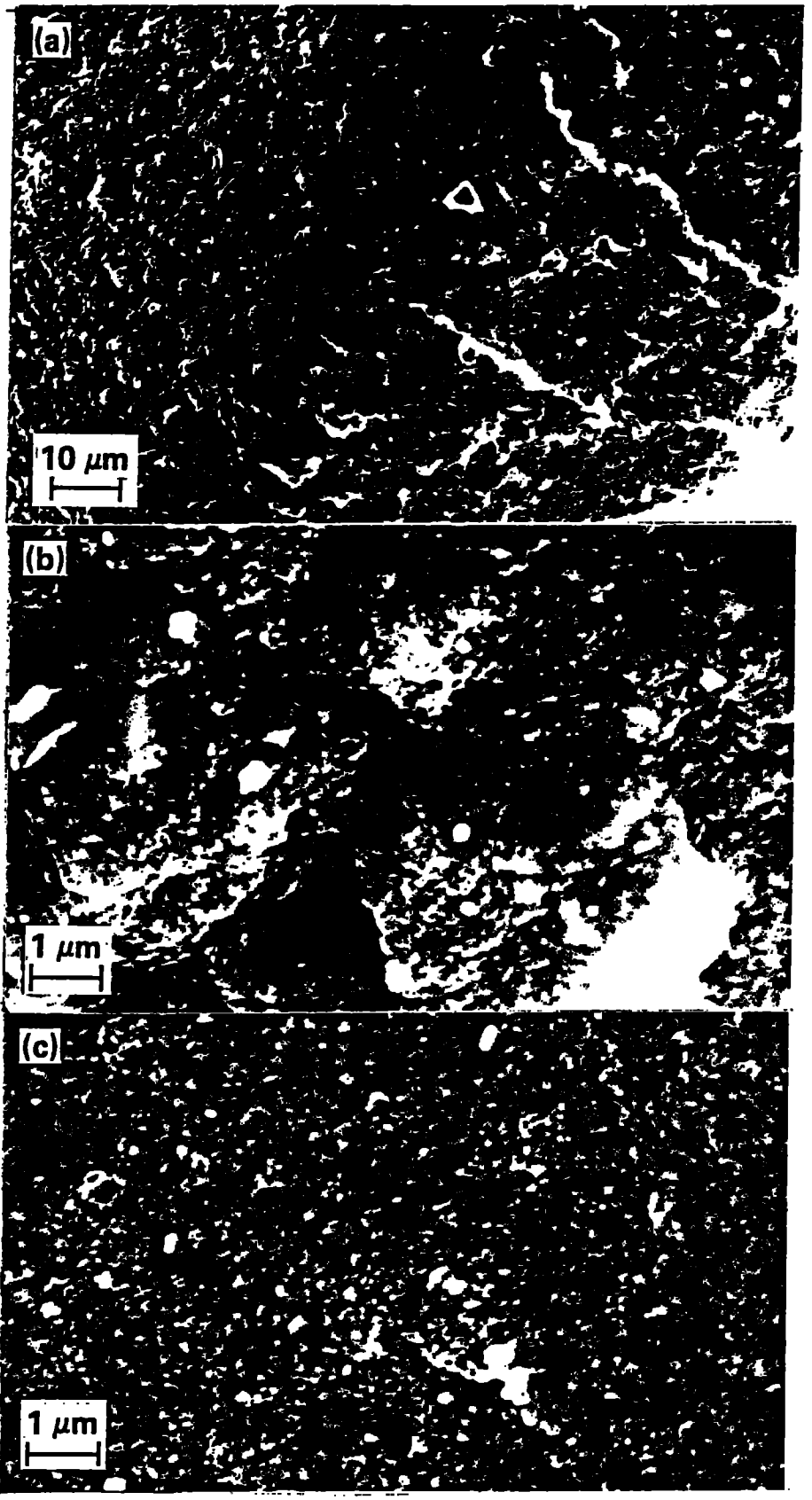

Figure 8: SBR-35 sample cycled at 100° C for 10 cycles at 0 to 10.07 MPa (1.46 ksi) and failed on cycling: (a) Initiation site with no detectable flaw, and part of inner bands (see Figure 11.b); (b) Relatively rough surface at initiation site; (c) Relatively smooth surface in fast-fracture region. Note both (b) and (c) exhibit knobs typical of the basic fracture units

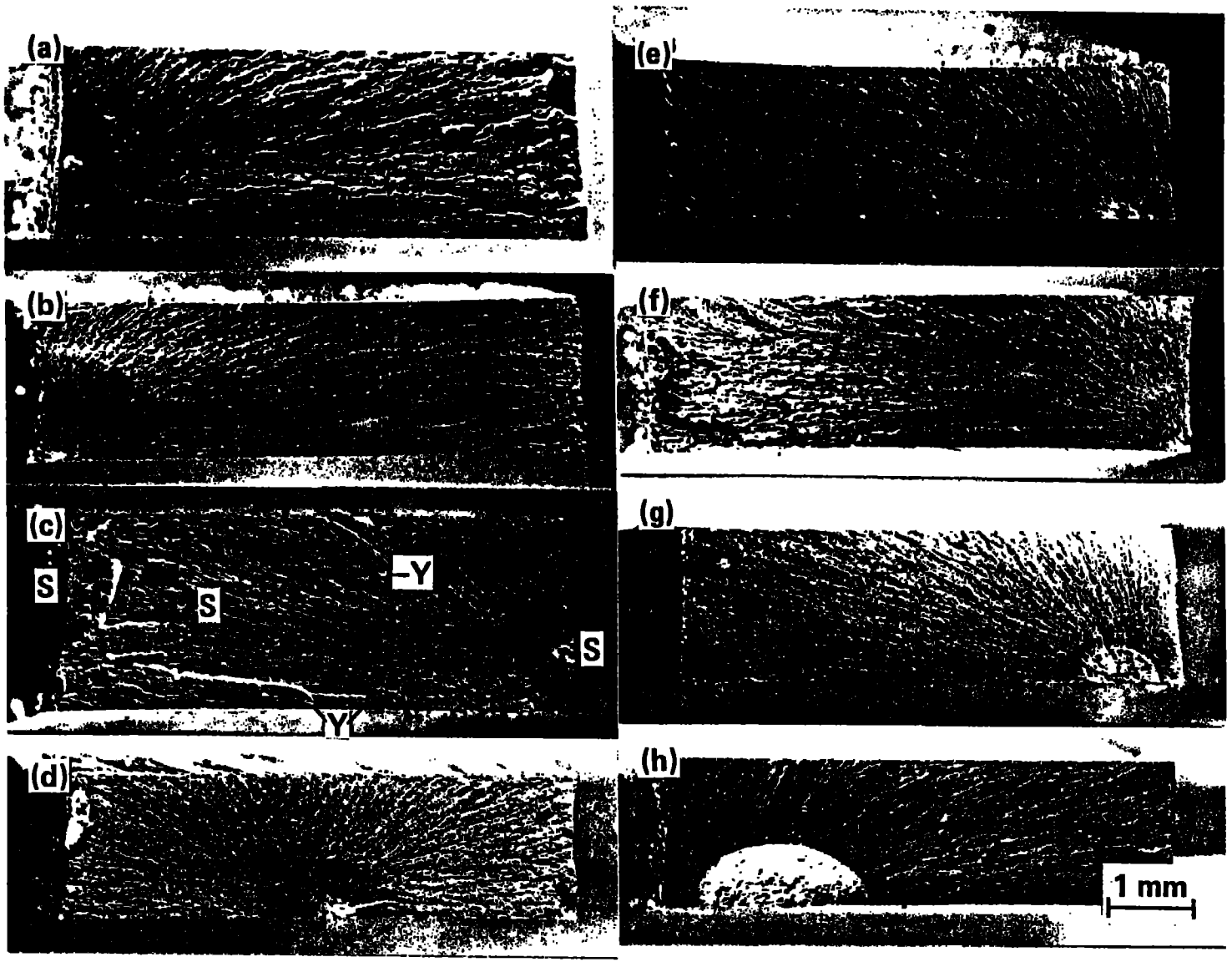

Figure 9: Low magnification fractographs of SBR-35 samples fractured at 22° C illustrating effect of cycling stress and degree of damage on morphologies. Cycle stress, number of cycles, residual strength, respectively, as follows: (a) 0, 0, 26.0 MPa (3.77 ksi); (b) 5.73 MPa (831 pis), 100, 25.0 MPa (3.62 ksi); (c) 10.9 MPa (1.59 ksi), 100, 23.2 MPa (3.37 ksi); (d) 14.4 MPa (2.09 ksi), 100, 24.0 MPa (3.48 ksi); (e) 21.6 MPa (3.13 ksi), 34, 0; (f) 16.1 MPa (23.5 ksi), 100, 23.6 MPa (3.43 ksi); (g) 16.5 MPa (2.39 ksi), 100, 18.2 MPa (2.64 ksi); (h) 16.8 (2.44 ksi), 83, 0

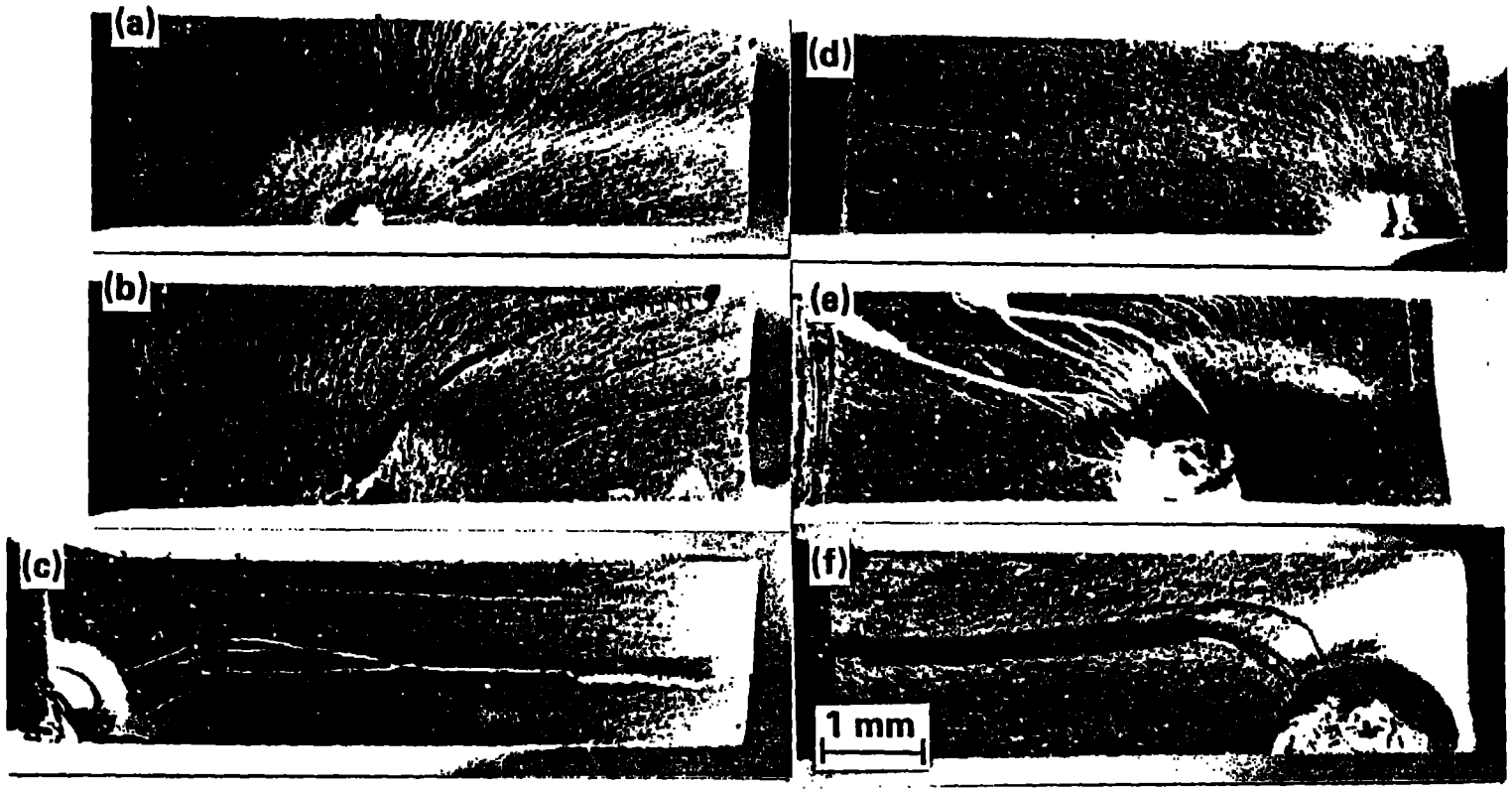

Figure 10: Low magnification fractographs of SBR-35 samples fractured at 100° C illustrating effect of cycling stress and degree of damage on morphologies. Cycle stress, number of cycles, residual strength, respectively, as follows: (a) 0, 0, 16.2 MPa (2.35 ksi); (b) 2.92 MPa (424 psi), 100, 14.2 MPa (2.06 ksi); (c) 10.0 MPa (1.46 ksi), 10, 0; (d) 6.07 MPa (881 pis), 100, 11.2 MPa (1.63 ksi); (e) 5.75 MPa (834 psi), 100, 7.41 MPa (1.08 ksi); (f) 6.05 MPa (878 psi), 31, 0

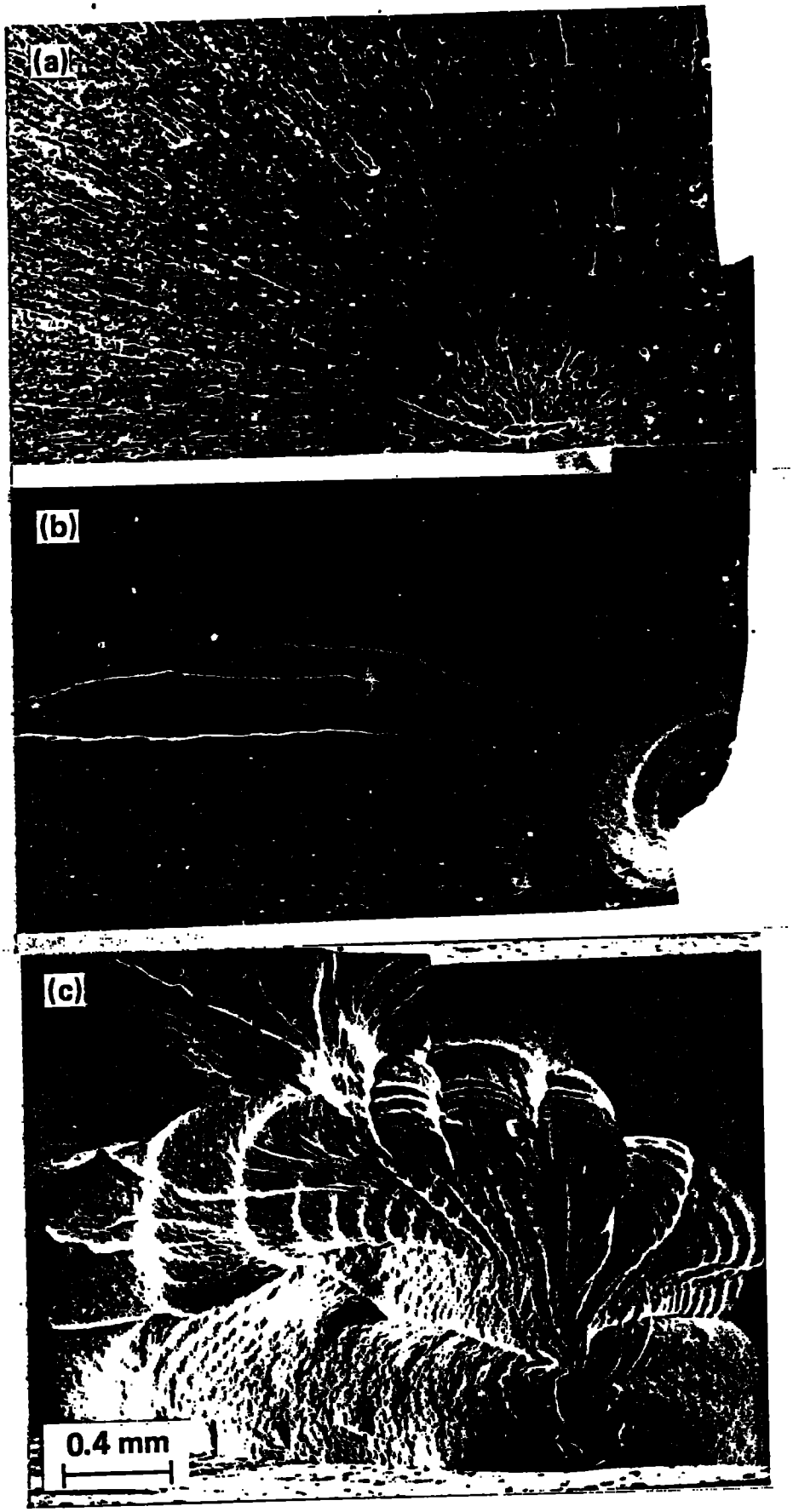

Figure 11: Initiation sites of SBR-35 samples cycled at three different temperatures: T, cycle stress, number of cyles to failure, respectively, as follows: (a) 22° C, 21.6 MPA (3.13 ksi), 34; (b) 100° C, 10.04 MPa (1.46 ksi), 10; (c) 140° C, 3.94 MPa (571 psi), 65. Note increase in band widths with increase fatigue-tear propagation

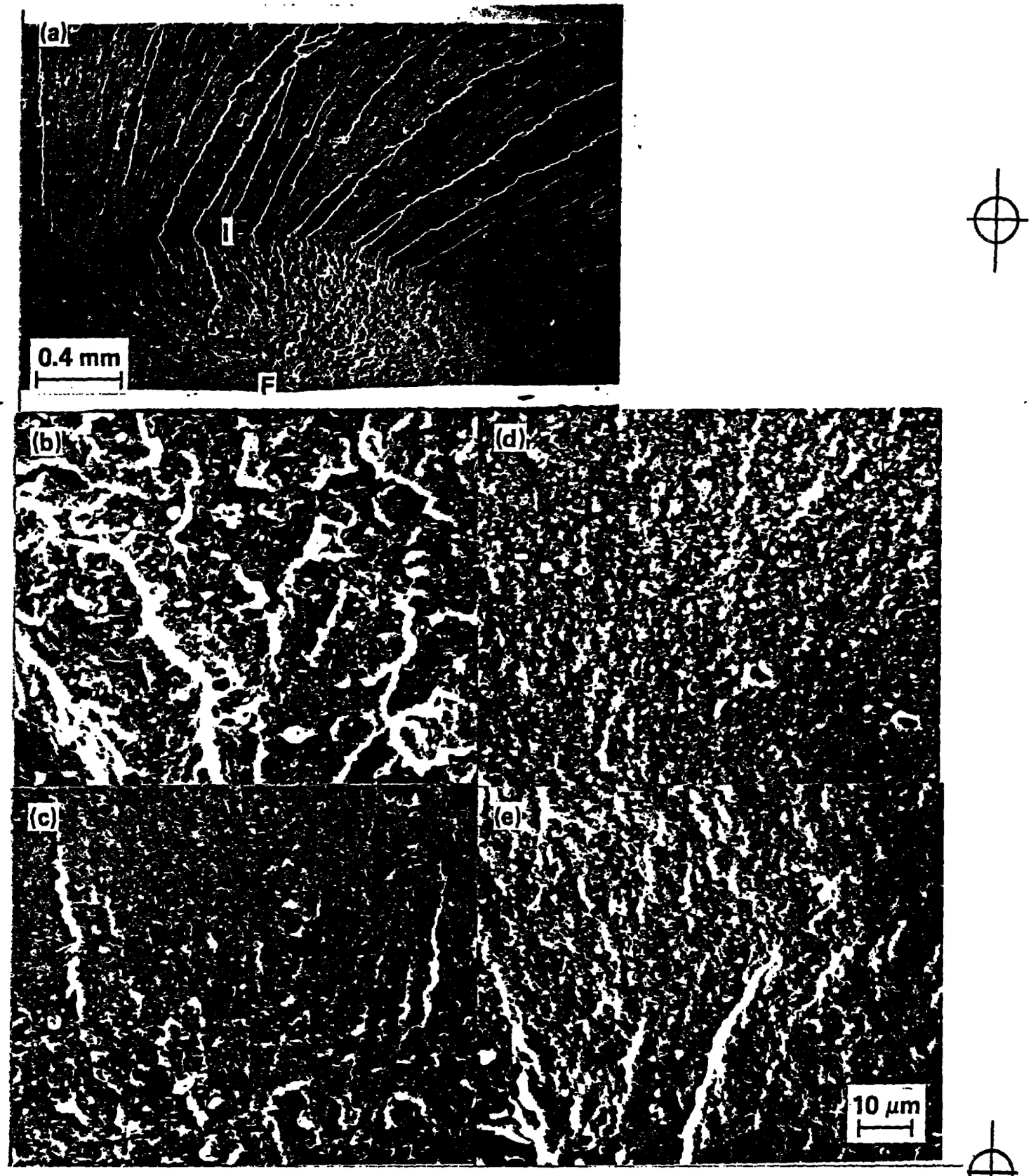

Figure 12: Differences in tear morphologies in banded region for SBR-35 samples cycled at three different temperatures: T, cylce stress, number of cycles, residual strength, respectively, as follows: (a), (b), and (c) 22° C, 16.8 MPa (2.44 ksi), 83, 0; (d) 100° C, 2.92 ksi (424 psi), 100, 14.2 MPa (2.06 ksi); (e) 140° C, 1.25 MPa (181 psi), 100, 10.89 MPa (1.58 ksi); View (b) is of area I and (c) is of area F in View (a); Views (b), (d), and (e) are taken just above initiation flaw.

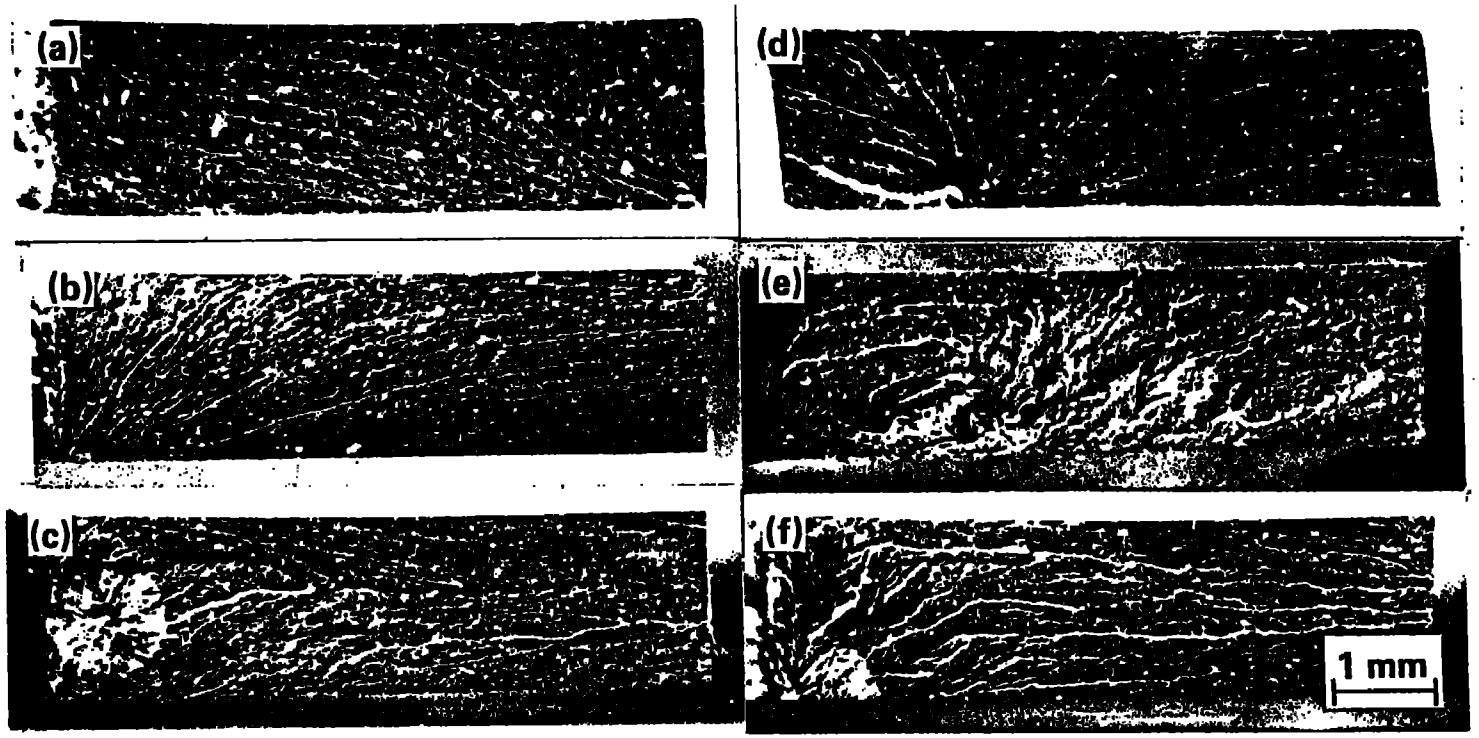

Figure 13: Low magnificiation fractographs of SBR-15 samples fractured at 100° C illustrating effect of cycling stress and degree of damage on morphologies: Cycle stress, number of cycles, residual strength, respectively, as follows: (a) 0, 0, 4.72 MPa (684 psi); (b) 1.32 MPa (192 psi), 100, 4.27 MPa (619 psi); (c) 1.79 MPa (260 psi), 95, 0; (d) 0, 0, 3.83 MPa (556 psi); (e) 1.36 MPa (197 psi), 50, 0; (f) 1.80 MPa (261 psi), 35, 0

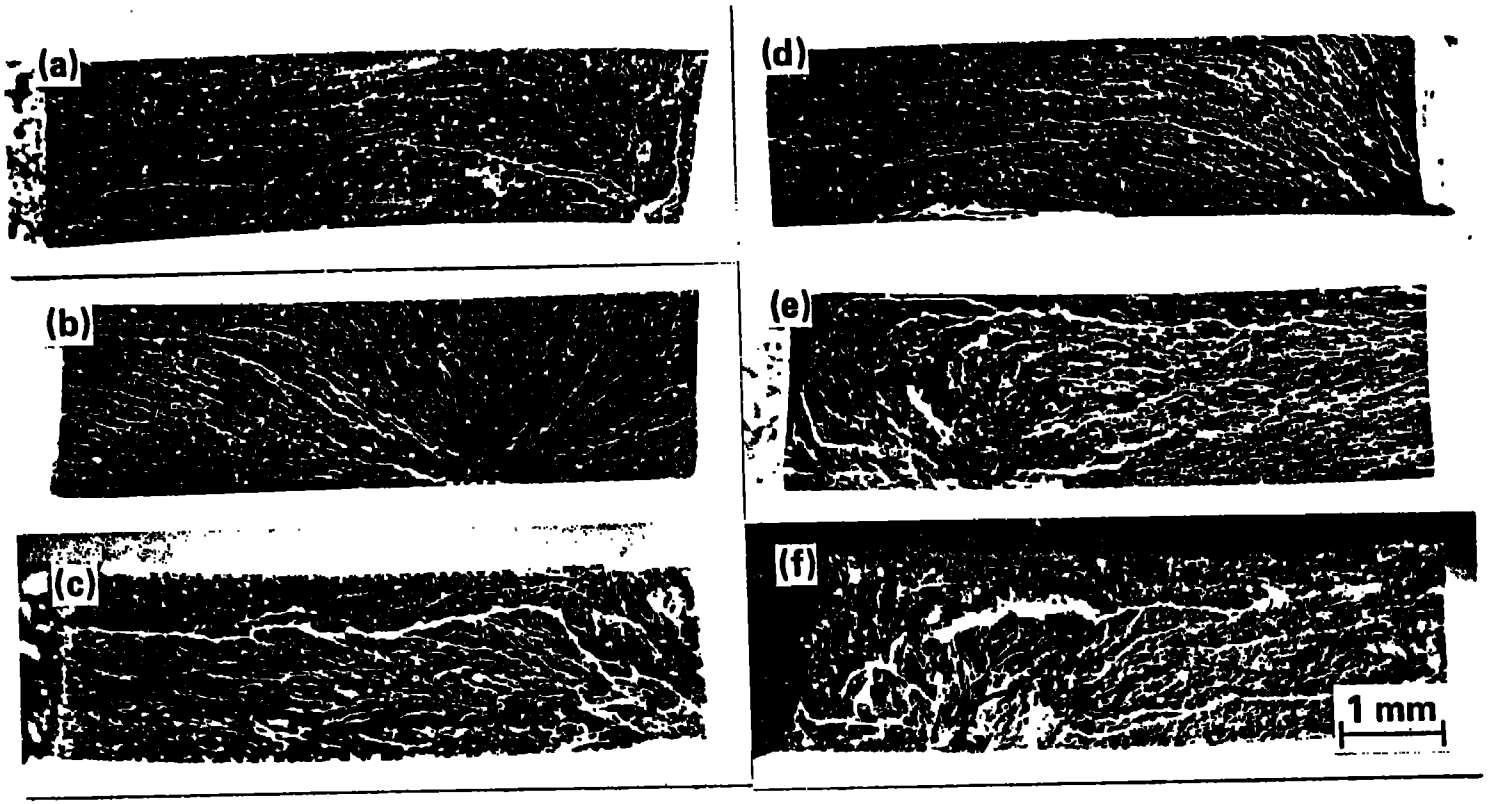

Figure 14: Low magnification fractographs of SBR-15 samples fractured at 140° C illustrating effect of cycling stress and degree of damage on morphologies: Cycle stress, number of cycles, residual strength, respectively, as follows: (a) 0, 0, 2.71 MPa (393 psi); (b) 1.17 MPa (169 psi), 100, 2.19 MPa (317 psi); (c) 1.45 MPa (210 psi), 21, 0; (d) 0, 0, 2.41 MPa (350 psi); (e) 1.12 MPa (163 psi), 80, 0; (f) 1.45 MPa (210 psi), 2, 0